Available online at www.sciencedirect.com

SciVerse ScienceDirect

Annals of Diagnostic Pathology 16 (2012) 459 – 469

Annals of DIAGNOSTIC PATHOLOGY

Biphasic alveolosquamoid renal carcinoma: a histomorphological, immunohistochemical, molecular genetic, and ultrastructural study of a distinctive morphologic variant of renal cell carcinoma☆,☆☆

Fredrik Petersson, MD, PhD[a,b], Stela Bulimbasic, MD, PhD[c], Ondrej Hes, MD, PhD[a,*], Pavol Slavik, MD[d], Petr Martínek, MSc[a], Michal Michal, MD[a], Barbora Gomolčáková[e], Milan Hora, MD, PhD[f], Ivan Damjanov, MD, PhD[g]

[a]*Department of Pathology, Charles University in Prague–Faculty of Medicine in Plzen, Plzen, Czech Republic*
[b]*Department of Pathology, National University Health System Hospital, Singapore, Singapore*
[c]*Department of Pathology, University Hospital Dubrava, Zagreb, Croatia*
[d]*Department of Pathology, University Hospital Martin, Martin, Slovak Republic*
[e]*Department of Pathology, Cytopathos, Bratislava, Slovak Republic*
[f]*Department of Urology, Charles University in Prague–Faculty of Medicine in Plzen, Plzen, Czech Republic*
[g]*Department of Pathology, University of Kansas, Kansas City, KS, USA*

Abstract Only a few cases of sarcomatoid renal cell carcinomas (RCCs) with squamous differentiation have been published. We present 2 RCCs exhibiting a hitherto not reported biphasic neoplastic cell population exhibiting a predominantly alveolar architecture where squamoid differentiation was identified in one of the neoplastic cell populations. None of the tumors showed chromophobe features or any evidence of sarcomatoid transformation. The tumors arose in 2 adult patients and were characterized by routine histology, immunohistochemistry, ultrastructure, array comparative genomic hybridization, confirmatory fluorescent in situ hybridization, and loss of heterozygosity analysis. Tumors measured 3 and 4 cm and were located within the renal parenchyma and had no pelvicalyceal connection. Both tumors were composed of a distinctly dual-cell population. The larger tumor cells displayed squamoid features and formed round well-demarcated solid alveolated islands that, in large parts, were surrounded by a smaller neoplastic cell component. The squamoid cells were immunoreactive for cytokeratins (CKs) (AE1-AE3, Cam 5.2, CK5/6, CK7, and CK20), epithelial membrane antigen, racemase/AMACR, and carboanhydrase IX (in 1 case focally). The small cell population was positive for CK7, epithelial membrane antigen, and racemase/AMACR, whereas CK20, AE1-3, and carboanhydrase IX were negative. CD10 was focally positive in the large squamoid cells in 1 case. Cathepsin K, E-cadherin, and CD117 displayed focal positivity in 1 case. Vimentin, RCC marker, parvalbumin, S100 protein, S100 A1, p63, p53, CDX2, uroplakin III, HMB45, TFE3, WT1, synaptophysin, chromogranin A, thyroglobulin, and TTF1 were negative. The proliferative activity (Ki-67) was low (1%) in the small cell component in both cases, whereas the large neoplastic tumor cells displayed a significantly higher proliferation (20%-35%). Ultrastructurally, desmosomes and tonofilaments were identified in the large tumor cells, confirming squamoid differentiation in a subset of tumor cells. Array comparative genomic hybridization of 1 analyzable case (confirmed with fluorescent in situ hybridization and loss of heterozygosity analysis) revealed partial or complete losses of chromosomes 2, 5, 6, 9, 12, 15, 16, 17, 18 and 22, (including biallelic loss of *CDKN2A* locus) and partial gains of chromosomes 1, 5, 11, 12 and 13. Follow-up at 6 years showed no recurrence or metastasis in 1 patient. The other (male) patients had a subcutaneous

☆ The study was supported by Czech Government grant agency (IGA NT12010-4) and by Charles University Grant (SVV 264805/2012).
☆☆ The authors declare that they have no conflict of interest.

* Corresponding author. Department of Pathology, Charles University, Medical Faculty and Charles University Hospital Plzen, Alej Svobody 80, 304 60 Pilsen, Czech Republic. Tel.: +420377104643; fax: +430377104650.
E-mail address: hes@medima.cz (O. Hes).

1092-9134/$ – see front matter
http://dx.doi.org/10.1016/j.anndiagpath.2012.08.007

metastasis at presentation, but during a 1-year follow-up no evidence of recurrence or further metastatic events have been documented. Our data indicate that biphasic alveolosquamoid renal carcinoma is a unique and distinctive tumor. The large squamoid and small tumor cells have overlapping but still distinctive immunohistochemical patterns of protein expression. Multiple chromosomal aberrations were identified, some of them located in regions with known tumor suppressor genes and oncogenes.

Keywords: Kidney; Renal cell carcinoma; Biphasic; Squamous; Squamoid; Alveolosquamoid carcinoma; Comparative genomic hybridization; Immunohistochemistry; Ultrastructure

1. Introduction

Squamous differentiation is rarely seen in renal cell carcinomas (RCCs). To date, only few such cases have been published [1,2]. In all reported cases of RCCs with squamous differentiation, this has consistently been found in the setting of sarcomatoid dedifferentiation/transformation of chromophobe RCCs (CHRCCs). In this study, we present 2 RCCs exhibiting a heretofore undescribed biphasic cellular composition featuring a predominantly alveolar arrangement of tumor cells and with a squamoid type of differentiation in 1 of the 2 cell types. The tumors did not show any histologic evidence of sarcomatoid transformation.

2. Materials and methods

Both cases were sent to one of the authors (O.H.) for second opinion (case 1 from Kansas City University Hospital and case 2 from Martin University Hospital, Slovak Republic). Tissue for light microscopy had been fixed in 4% formaldehyde and embedded in paraffin using routine procedures. Five-micrometer-thin sections were cut and stained with hematoxylin and eosin.

2.1. Immunohistochemistry

The following primary antibodies were used: epithelial membrane antigen (EMA) (E29, monoclonal; DakoCytomation, Carpenteria, California; 1:1000), cytokeratins (CKs) Cam 5.2 (monoclonal; Becton-Dickinson, San Jose, California; 1:200) and AE1-AE3 (monoclonal; BioGenex, San Ramon; California; 1:1000), CK5/6 (D5/16B4, monoclonal; DakoCytomation; 1:100), CD10 (56C6; Novocastra, Burlingame, California; 1:20), CK7 (OV-TL12/30, monoclonal; DakoCytomation; 1:200), CK20 (M7019, monoclonal; DakoCytomation; 1:100), racemase/AMACR (P504S, monoclonal; Zeta, Sierra Madre, California; 1:50), vimentin (D9, monoclonal; NeoMarkers, Westinghouse, California; 1:1000), parvalbumin (PA-235, monoclonal; Sigma-Aldrich, St Luis, Missouri; 1:500), antimitochondrial antigen (MIA) (113-1, monoclonal; BioGenex; 1:800), Ki-67 (MIB1, monoclonal; DAKO, Glostrup, Denmark; 1:1000), c-kit (CD117, polyclonal, 1:300), E-cadherin (12H6, monoclonal; Zymed, San Francisco, California; 1:200), and carbonic anhydrase IX (rhCA9, monoclonal; RD systems, Abingdon, GB, UK; 1:100). Renal cell carcinoma marker (SPM 314, monoclonal; DAKO; 1:50), p63 (4A4, monoclonal, RTU; Ventana, Tucson, Arizona), p53 (DO-7, monoclonal; DakoCytomation; 1:30), CDX2 (CDX2-88, monoclonal; Biogenex; 1:150), antimelanosome (HMB45, monoclonal; DakoCytomation; 1:200), uroplakin 3 (SFI-1; Abcam, Cambridge, UK; 1:50), TFE3 (polyclonal; Abcam; 1:100), cathepsin K (3F9, monoclonal; Abcam; 1:100), WT1 (GF-H2, monoclonal; DakoCytomation; 1:150), synaptophysin (polyclonal; Thermo Scientific, Cheshire, UK; 1:400), chromogranin A (DAK A3, monoclonal; DakoCytomation; 1:300), S100 (polyclonal; DakoCytomation; 1:400), S100A1 (polyclonal; GenWay, San Diego, California; 1: 100), TTF-1 (SPT24, monoclonal; Novocastra, Newcastle, UK; 1:400), thyroglobulin (polyclonal, RTU; DakoCytomation), OCT3/4 (N1NK, monoclonal; Novocastra; 1:80), nanog (polyclonal; RD Systems; 1:100), and SALL4 (GE3, monoclonal, 1:600; Sigma-Aldrich; 1:800). The primary antibodies were visualized using the supersensitive streptavidin-biotin-peroxidase complex (BioGenex). Appropriate positive controls were used.

2.2. Ultrastructural study

Small pieces of the formaldehyde fixed wet tissue from case 1 were postfixed in glutaraldehyde and routinely processed for electron microscopy. Neoplastic, paraffin-embedded tissue from case 2 was deparaffinized and was further routinely processed for ultrastructural analysis.

3. Molecular genetic study

3.1. DNA extraction

DNA from formalin-fixed, paraffin-embedded tumor and nontumor tissues of the patients was extracted using NucleoSpin Tissue Kit (Macherey Nagel, Düren, Germany), according to manufacturer's instructions.

Concentration and purity of isolated DNA were measured using Nanodrop ND-1000 (NanoDrop Technologies Inc, Wilmington, Delaware). Integrity and amplifiability of isolated DNA were examined by amplification of control genes in a multiplex polymerase chain reaction (PCR) [3].

3.2. Array comparative genomic hybridization

3.2.1. Sample preparation and labeling

Two micrograms of DNA was diluted in 80 μL H_2O and sonicated for 10 seconds at 10% amplitude with Pulse On for 0.5 second and Pulse Off for 0.5 second on a Branson 450 sonicator equipped with a tapered microtip (Branson, Danbury, Connecticut). One microgram of sonicated DNA of tumor and nontumor sample was mixed with Cy3 and Cy5 random-labeled 7mer primers, respectively. The samples were denatured and then incubated for 2 hours at 37°C in a thermocycler protected from light with dNTP/Klenow Master Mix (Roche Nimblegen Inc, Madison, Wisconsin). One hundred units of Klenow Fragment 3′-5′ exo (NEB, Ipswich, Massachusetts) was used per sample. The reaction was stopped by addition of 0.5 M EDTA, and labeled samples were purified using isopropanol precipitation. Six micrograms of the tumor and nontumor samples was combined in 1 tube dried and resuspended in 5 μL of nuclease-free H_2O.

3.2.2. Hybridization

The hybridization protocol was performed using MAUI Hybridization system (BioMicro, Salt Lake City, Utah) and required adhering a NimbleChip X1 mixer to the microarray slide NimbleGen 385K Human comparative genomic hybridization (CGH) WG-T v2.0, build: HG18, NCBI 36, Median Probe Spacing 7073 base pairs (Roche). The hybridization master mix solution was prepared using components from a NimbleGen Hybridization Kit (Roche) according to the manufacturer's protocol. Hybridization solution and samples were mixed, denatured, and loaded into the fill port of a mixer. Then the samples were hybridized for 20 hours at 42°C in the mix mode B. Posthybridization washing was done using Nimblegen buffers with increasing stringency (Roche).

3.2.3. Scan and gridding

Microarrays were scanned with InnoScan 700 (Innopsys, Carbonne, France) at a resolution of 3 μm. Image analysis was performed using NimbleScan 2.5 software (Roche) according to appropriate .ndf file.

3.2.4. Data analysis

The data analysis was also processed in NimbleScan 2.5 (Roche) using CGH-segMNT Analysis. Prior to segmentation analysis, the qspline fit normalization, which compensates for inherent differences in signal between the 2 dyes, was applied [4]. The segMNT algorithm identifies copy number changes using a dynamic programming process that minimizes the squared error relative to the segment means. This procedure allows us to generate a list of candidate breakpoints, identify the best segmentation for each given number of breakpoints, and determine the number of segments to output results. The minimum segment difference in the log2 ratio that 2 segments must exhibit before they are identified as separate segments was set to 0.1. Minimum segment length was set to 2 probes. The stringency with which initial segment boundaries were selected was set to a maximal stringent value of 0.9999. Nonaveraged and 10× reduced averaging window segmentation was applied to raw data, which gave us a data spacing of 7000 and 70 000 base pairs, respectively. As output, .gpr, .txt, and .pdf files were produced, which allowed us further analysis in respect to HG18 annotation tracks using SignalMap (Roche) or any other text editor or tab processor.

Cutoff values for log2 ratio were set to −0.193 for loss and +0.170 for gain [5].

3.3. Fluorescent in situ hybridization

A 4-μm-thick section was placed onto a positively charged slide. The hematoxylin and eosin–stained slide was examined for determination of areas for cell counting. The unstained slide was routinely deparaffinized and incubated in the 1× Target Retrieval Solution Citrate pH 6 (DAKO) for 40 minutes at 95°C and subsequently cooled for 20 minutes at room temperature in the same solution. The slide was washed in deionized water for 5 minutes, and tissue was covered with the Proteinase K (20 mg/mL) (SERVA, Heidelberg, Germany) for 6 minutes at room temperature. The slide was then placed into deionized water for 5 minutes, dehydrated in a series of ethanol solution (70%, 85%, 96% for 2 minutes each), and air-dried. CDKN2A/CEP 9 fluorescent in situ hybridization Probe Kit (VYSIS/Abbott Molecular, Des Plaines, Illinois) was mixed with water and LSI/WCP Hybridization buffer (VYSIS) in a 1:2:7 ratio. An appropriate amount of probe mix was applied on specimen, covered with a glass coverslip, and sealed with rubber cement. The slide was incubated in the ThermoBrite instrument (StatSpin/Iris Sample Processing, Westwood, Massachusetts) with codenaturation parameters 85°C for 8 minutes and hybridization parameters 37°C for 16 hours. Rubber-cemented coverslip was then removed, and the slide was placed in posthybridization wash solution (2× SSC/0.3% NP-40) at 72°C for 2 minutes. The slide was air-dried in the dark, counterstained with DAPI I (VYSIS), covered with coverslip, and immediately examined.

3.4. Fluorescent in situ hybridization interpretation

The section was examined with an Olympus BX60 fluorescence microscope using a 100× objective and filter sets Triple Band Pass (DAPI/Spectrum Green/Spectrum Orange) and Single Band Pass (Spectrum Green and Spectrum Orange). Scoring of aneuploidy was performed by counting the number of fluorescent signals in 100 randomly selected nonoverlapping tumor cell nuclei. The slide was independently enumerated by 2 observers (P.M. and B.G.). Nullisomy for studied chromosome was defined as the presence of zero signal per cell in more than 10% nuclei (in nuclei with at least 1 signal of control probe per nucleus).

3.5. Loss of heterozygosity analysis

Loss of heterozygosity (LOH) analysis was performed using selected STR markers included in uniSTS database. Polymerase chain reaction was performed in 25-μL reaction volumes consisting of 100 ng of DNA, 12.5 μL of FastStart PCR Master mix (Roche), 10 pmol of forward (fluorescent labeled), and reverse primer diluted in distilled water. The amplification program comprised 4 minutes of initial denaturation at 95°C, followed by 35 cycles of denaturation at 95°C for 1 minute, annealing at 55°C for 1 minute, and extension at 72°C for 1 minute. The program ended with final extension at 72°C for 7 minutes. Polymerase chain reaction products were checked with 2 % agarose gel electrophoresis and if necessary diluted with distilled water. One microliter of successfully amplified PCR products was mixed with 0.3 μL Gene Scan-500LIZ Size Standard (Applied Biosystems), 25 μL of HiDiFormamide (Applied Biosystems), and run on an automated genetic analyzer ABI Prism 3130xl (Applied Biosystems) at a constant voltage of 15 kV for 20 minutes. Intensity of fluorescence was measured. Height ratio of 2 alleles of tumor sample in relative fluorescence units was divided by ratio of 2 alleles of nontumor sample respecting the order of alleles. Cutoff values for LOH positive markers were set to less than 0.75 and more than 1.33 [6].

4. Results

4.1. Clinical data

4.1.1. Case 1

A 54-year-old woman underwent partial resection of the right kidney for an asymptomatic tumor, which was incidentally discovered on ultrasonography performed in conjunction with a traffic accident. The patient is alive and well 6 years after nephrectomy.

4.1.2. Case 2

A 68-year-old male patient underwent surgical excision of a skin tumor on the dorsal aspect of the neck. Histologic examination revealed a carcinoma of uncertain origin, and the possibility of a metastasis was raised. Subsequently, a tumor of the right kidney was detected on a computed tomography scan. An open radical nephrectomy was performed. At 1-year follow-up, no evidence of recurrence or further metastatic events have been documented.

4.2. Pathological findings

4.2.1. Gross pathology

Case 1. The tumor measured 3.0 cm in largest dimension, was well circumscribed, and was located in the cortex with no connection to the pelvicalyceal system. Cut sections were solid with a gray to tan color. Necrosis was not evident.

Case 2. The tumor was solid measuring 3.7 cm in maximum dimension. The tumor was located in the cortical area of the upper pole and was focally not well demarcated from the renal parenchyma. The renal capsule and the sinus were not involved by the tumor. Cut sections of the tumor had a grayish hue. Small foci of necrosis were seen. No relation to the pelvicalyceal structures was noted.

4.2.2. Light microscopy

On light microscopic examination, both tumors were composed of 2 distinctive neoplastic cell populations, which were arranged in various patterns, including a variety of complex lace-like patterns and solid, alveolated aggregates composed of larger, polygonal, neoplastic cells (Fig. 1A + B). These alveolar nests were rimmed by distinctly smaller tumor cells (Fig. 2). The larger tumor cells in the centers of the alveolar structures displayed variable degrees of acantholysis-like discohesion (Fig. 3). The small tumor cells were mostly cuboidal and displayed a high nuclear-to-cytoplasmatic ratio. The nuclei were round to oval with small to inconspicuous nucleoli, and the limited cytoplasm was pale to lightly eosinophilic. However, in both tumors, the small cell

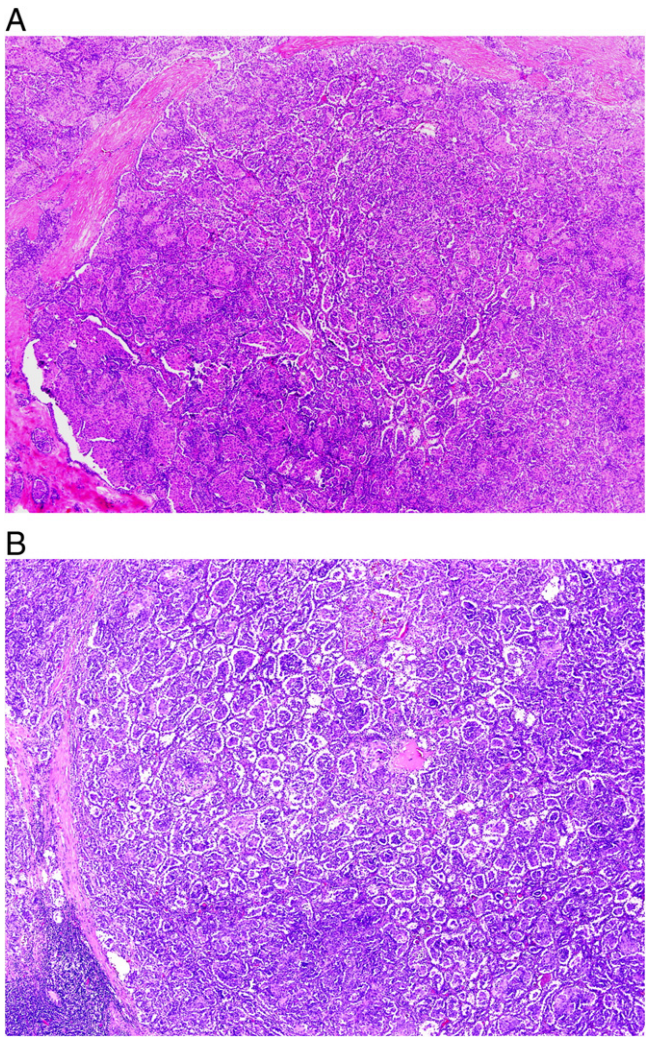

Fig. 1. (A + B) Both tumors were composed of 2 distinctive neoplastic cell populations, which were arranged in complex lace-like patterns and solid, alveolated aggregates composed of larger, polygonal, neoplastic cells.

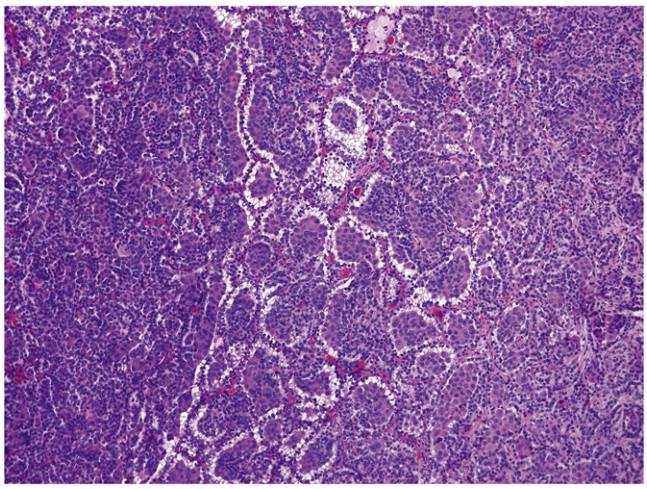

Fig. 2. Alveolar nests composed of large squamoid cells were rimmed by distinctly smaller tumor cells.

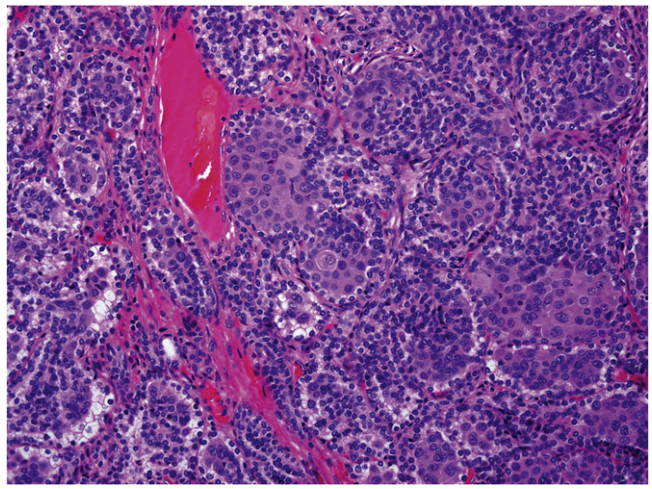

Fig. 4. The cells had marked cell membranes and were frequently displayed a pavement-like arrangement.

population contained occasional larger, more pleomorphic cells with more prominent nucleoli. Focal intranuclear inclusions were seen in case 1. A minor proportion (2%-3%) of the small neoplatic cells in case 2 displayed some resemblance to oncocytes. These oncocyte-like cells were surrounded by a loose, cell-poor, edematous stroma.

The large tumor cell population was polygonal in shape and had abundant, dense eosinophilic cytoplasm, which, in many areas, displayed a squamoid appearance. The cells had marked cell membranes and frequently showed a pavement-like arrangement (Fig. 4). However, no definitive intercellular briges or bona fide keratin pearls were identified. The nuclei were pleomorphic and contained mostly one central large nucleolus. These nuclear changes were most prominent in case 2 (Fig. 5). Mitotic activity was almost exclusively seen in the large cell component. No abnormal mitotic figures were found.

The previously described alveolated pattern was the predominant architectural arrangement of cells in case 1, whereas it was more focal in case 2. In addition, the neoplastic cells in case 1 exhibited a more solid and sheet-like growth pattern with areas composed of small cells containing larger islands and irregular cords of larger polygonal cells. A very small proportion, accounting for less than 2% of the tumor, revealed papillary structures lined by the small neoplastic cell component. The predominant growth pattern in case 2 was that of large sheets and irregular nests composed of polygonal cells surrounded by a rim of a single to 2 layers of small cells. In areas where the large cells predominated, a few microscopic foci of necrosis were identified (not present in case 1).

An interesting phenomenon was the focal presence of emperipolesis, that is, large tumor cells with phagocytosed cellular material (Fig. 6).

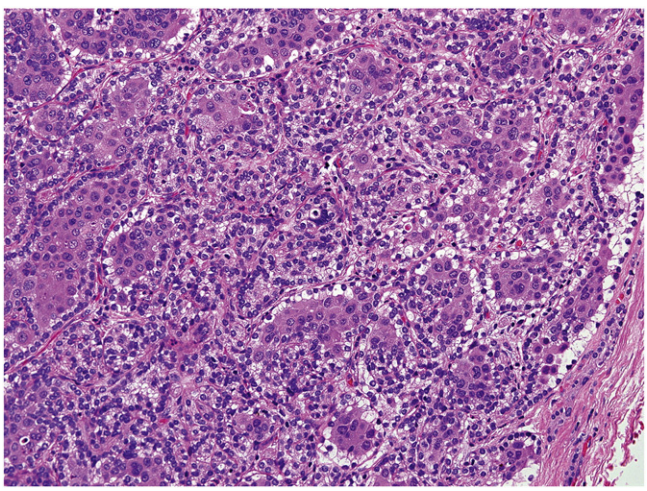

Fig. 3. The larger tumor cells in the centers of the alveolar structures displayed variable degrees of acantholysis-like discohesion.

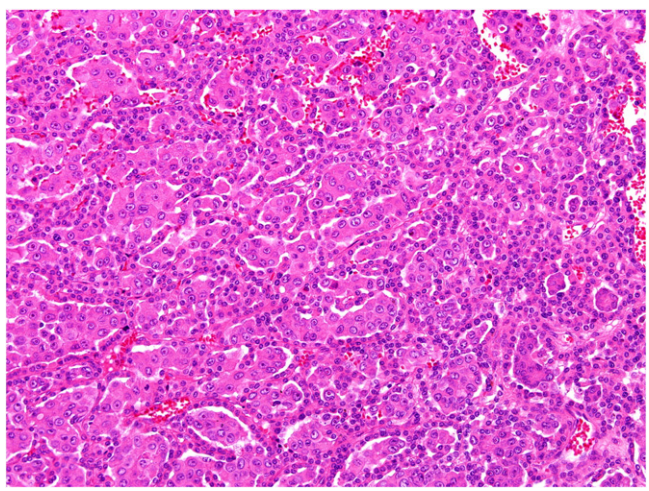

Fig. 5. The nuclei were pleomorphic and contained mostly one central large nucleolus.

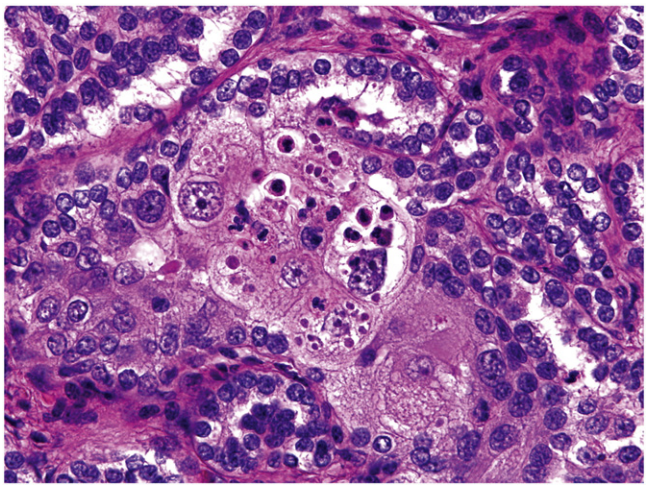

Fig. 6. An interesting phenomenon was the focal presence of emperipolesis.

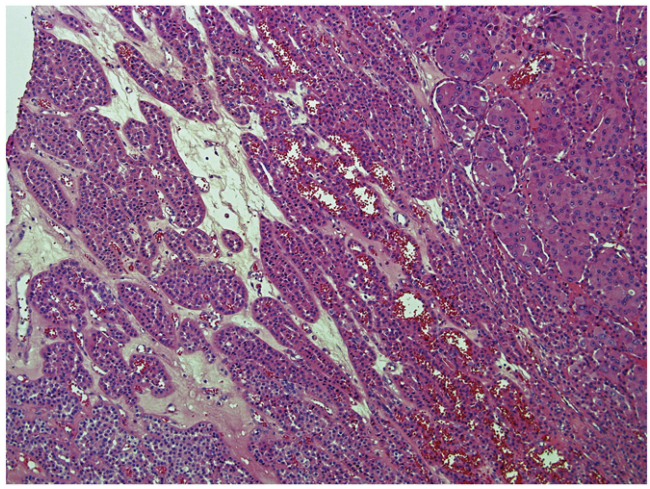

Fig. 7. In few small areas in case 2, neoplastic cells of intermediate size formed small alveolar nests imparting an oncytoma-like appearance.

An additional but only focal feature noted in case 2 was that the large tumor cells showed formation of lumina, which contained bluish mucoid material stained positive with Hale's colloidal iron (Fig. 7). In few small areas in case 2, neoplastic cells of "intermediate" size formed small alveolar nests imparting an oncytoma-like appearance (Fig. 8).

In both tumors, focal prominent fibrous/collagenous stroma was present (highlighted with Masson trichrome stain).

The nonneoplastic renal parenchyma was unremarkable in both cases, and no significant chronic tubulointerstitial or glomerular changes were seen. No dysplastic changes were seen in the urothelial lining of the renal pelvis in any of the cases.

The cutanous metastasis (case 2) was exclusively composed of the histologically obviously malignant large cell component.

4.3. Immunohistochemistry

The results of the immunohistochemical study are summarized in Table 1. Briefly, both the small and large cell components (in both cases) were positive for CK7 and EMA. Cytokeratins 20 and 5/6 showed diffuse positivity in the large cell component and very focal and weak immunoreactivity in the small tumor cells (Fig. 9). The large tumor cells were diffusely positive for AE1-3, whereas the smaller neoplatic cells were negative. Cam 5.2 was strongly positive in the large cells, whereas the smaller tumor cells revealed a variable (none to moderate) positivity, with most cells displaying some degree of (mostly weak) immunoreactivity. Positive reaction to CD10 was focal mild and cytoplasmic in the area with papillary structures in case 1. Focal moderate cytoplasmic immunoreactivity for CD10 was detected in the large cell component in case 2. Racemase/AMACR showed focal to moderate positivity in both components in case 1 and selectively in the large cells in case 2 (Fig. 10). The small cell component in case 2 exhibited focal moderate membranous positivity for E-cadherin and diffuse weak cytoplasmic immunoreactivity for CD117. The large cell component in case 2 showed focal moderate positivity for cathepsin K (Fig. 11). Both tumors were completely negative for RCC marker, uroplakin 3, vimentin, CDX2, WT-1, S100-A1, p63, p53, HMB-45, TFE3, synaptophysin, chromogranin A, S-100 protein, TTF-1, and thyroglobulin. Both tumors were completely negative for OCT3/4, nanog, and SALL4.

A granular cytoplasmic immunoreactivity for MIA with variable intensity was found in both cell types in both cases. This was significantly more prominent in the large, squamoid cell population where the granules displayed a larger and coarser quality than in the small neoplastic cell population. The minute oncocytoid foci in tumor 2 revealed diffuse cytoplasmic positivity.

The proliferative activity (MIB-1/Ki-67) in the small cell component in both cases was low (approximately 1%), whereas the large cell component showed increased proliferative activity: 20% and 35% in cases 1 and 2, respectively.

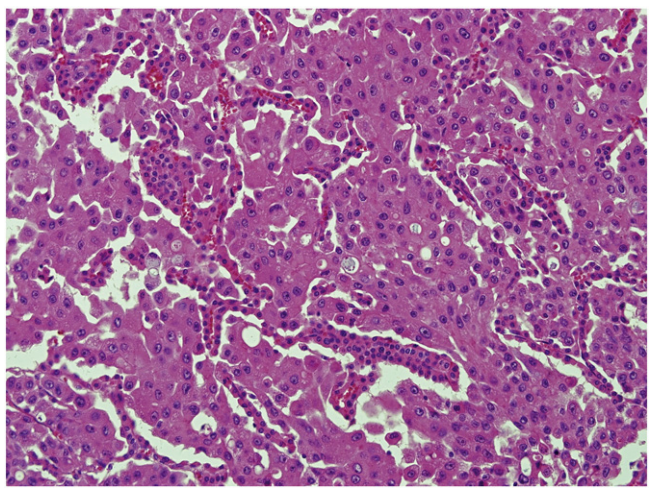

Fig. 8. The large tumor cells showed focal formation of lumina, which contained bluish mucoid material.

Table 1
Immunohistochemical features

Antibodies	CK AE1/3	CK7	CK20	CK5/6	EMA	CD10	RCC	AMACR	Vim	E-cadh	CAH9	Parv	c-kit	S-100 A1
Case 1														
Small cells	Neg	++	Neg	Foc +	++	Neg	Neg	Foc ++	Neg	Neg	Neg	Neg	Neg	Neg
Large cells	++	++	++	++	++	Neg	Neg	Foc +	Neg	Neg	++	Neg	Neg	Neg
Case 2														
Small cells	Neg	Foc ++	Neg	Neg	Foc +	Neg	Neg	Neg	Neg	Foc ++	Neg	Neg	foc+	Neg
Large cells	+++	+++	+++	+++	+	Foc +	Neg	Foc +/++	Neg	Neg	Foc single cell	Neg	Neg	Neg

Antibodies	p63	p53	CDX	Uropl III	HMB45	TFE3	Cath K	WT1	Syn	Chrom	S100	TTF1	T4	MIB
Case 1														
Small cells	Neg	Neg	Neg	Neg	Neg	Neg	Neg	Neg	Neg	Neg	Neg	Neg	Neg	1%
Large cells	Neg	Foc single cell	Neg	Neg	Neg	Neg	Neg	Neg	Neg	Neg	Neg	Neg	Neg	20%
Case 2														
Small cells	Neg	Neg	Neg	Neg	Neg	Neg	Neg	Neg	Neg	Neg	Neg	Neg	Neg	1%
Large cells	Neg	Foc single cell	Neg	Neg	Neg	Foc ++	Foc ++	Neg	Neg	Neg	Neg	Neg	Neg	35%

+, mild positivity; ++, moderate positivity; +++, strong positivity; AMACR, racemase; E-cadh, E-cadherin; CAH9, carboanhydrase IX; foc, focally; neg, negative; parv, parvalbumin; vim, vimentin; cath K, cathepsin K; T4, thyreoglobulin; uropl III, uroplakin III; CDX, CDX 2; syn, synaptophysin; chrom, chromogranin.

4.4. Ultrastructure

Squamoid differentiation was confirmed ultrastructurally by the presence of desmosomes and tonofilaments in the cytoplasm of the large tumor cell population (Fig. 12). A variable number of mostly damaged mitochondria were identified in both cell types. Although the material was not optimal, there were no cells seen with the cytoplasm packed with mitochondria. We were not able to identify abundant cytoplasmic microvesicles in any of the tumor cells. Occasional intracytoplasmic lumina lined by microvilli were found in some of the small tumor cells.

4.5. Molecular genetic study

Analysis of the neoplastic tissue of case 2 by array CGH revealed losses on chromosomes 2, 5, 6, 9, 12, 15,16, 17, 18, and 22, including biallelic loss of *CDKN2A* locus, and gains on chromosomes 1, 5, 11, 12, and 13 (Table 2), (Fig. 13). Owing to the poor quality of the DNA, the neoplastic tissue from case 1 was not analyzable.

4.6. Fluorescent in situ hybridization

Fluorescent in situ hybridization analysis confirmed biallelic loss in cytoband 9p21.3 where *CDKN2A* is located (45% [100]) in the neoplastic tissue from case 2 (Fig. 14). In nontumor tissue, a normal signal pattern was observed.

4.7. Loss of heterozygosity analysis

The changes found by array CGH in case 2 were, whenever it was possible, confirmed by LOH analysis with informative markers (Table 2).

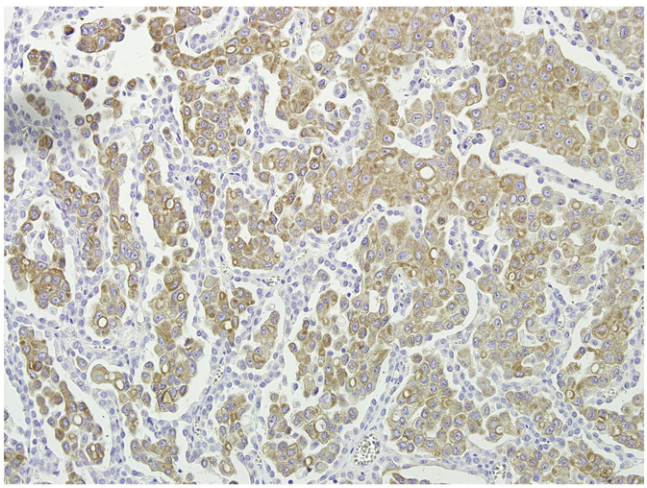

Fig. 9. CK 20 showed diffuse positivity in the large cell component and very focal and weak immunoreactivity in the small tumor cells.

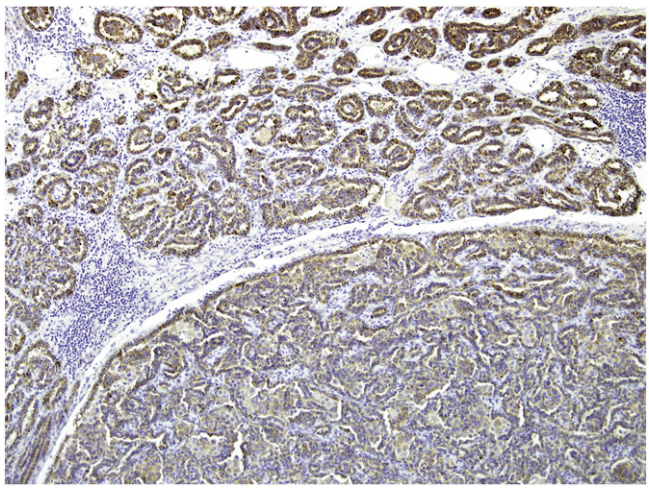

Fig. 10. Racemase/AMACR showed focal to moderate positivity in both components.

5. Discussion

In this study, we characterize in detail 2 renal carcinomas with histopathologic features that, to the best of our knowledge, have not been reported previously. There are only a few reports on RCCs exhibiting squamous differentiation, and all these tumors are CHRCCs with sarcomatoid transformation [1,2]. The cases presented herein differ from CHRCC by morphology, and also the immunohistochemical profile and ultrastructural features are not consistent with any unusual variant of CHRCC. In addition, although CHRCCs are characterized by multiple losses (monosomies) of chromosomes, the molecular genetic findings in the analyzed case in this study are different from profiles identified in CHRCCs. For example, of the 11 chromosomes that showed loss of genetic material in our analyzed case, only 4 occurred in chromosomes that frequently display losses in CHRCC. Moreover, our analyzed case also revealed gains of chromosomal material, which would be highly unusual for a CHRCC.

Microscopically, the tumors presented herein are characterized by the presence of a dual-cell population in varying proportions that exhibited a variety of growth patterns of which an alveolar arrangement of large tumor cells rimmed by the smaller neoplastic cells was the most frequently encountered. Notably, the larger cells displayed traditional histopathologic characteristics of malignancy (nuclear pleomorphism, large nucleoli). This is also supported by the significantly increased proliferation as measured immunohistochemically (which is in sharp contrast to that of the small cell component, which displayed an almost negligible proliferative activity) and also the fact that it was the large cell population that was exclusively encountered in the cutaneous metastasis (presenting symptom) in case 2. Immunohistochemically, these neoplasms were characterized by (1) positivity for CK7 and EMA in both the small and large cell components, (2) diffuse immunoreactivity for CK 20 and CK5/6 in the large cell component (with only very focal and weak immunoreactivity in the small tumor cells), and (3) complete absence of expression of RCC marker, vimentin, S100-A1, p63, HMB-45, TFE3, synaptophysin, chromogranin, S-100 protein, TTF-1, and thyroglobulin. The staining patterns for CD10, cathepsin K, racemase, E-cadherin, and c-kit/CD117 did not yield any consistent pattern of expression. However, it is interesting to note that the large cell component in 1 of the cases was clearly positive for cathepsin K, which has been thought of as a highly specific marker for the MiTF/TFE renal translocation carcinomas [7].

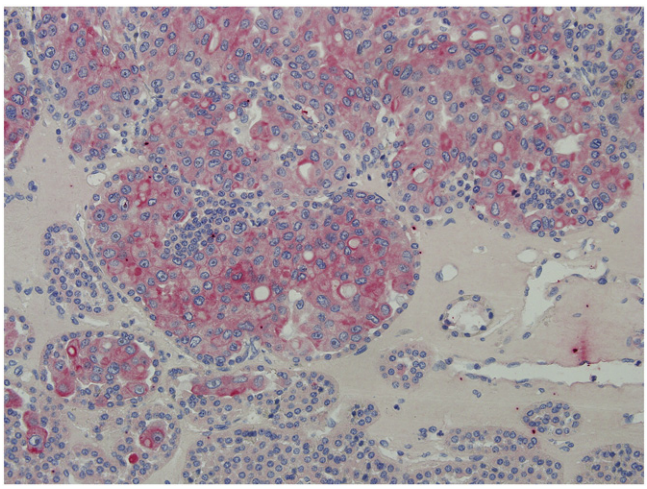

Fig. 11. The large cell component in case 2 showed focal to moderate positivity for cathepsin K.

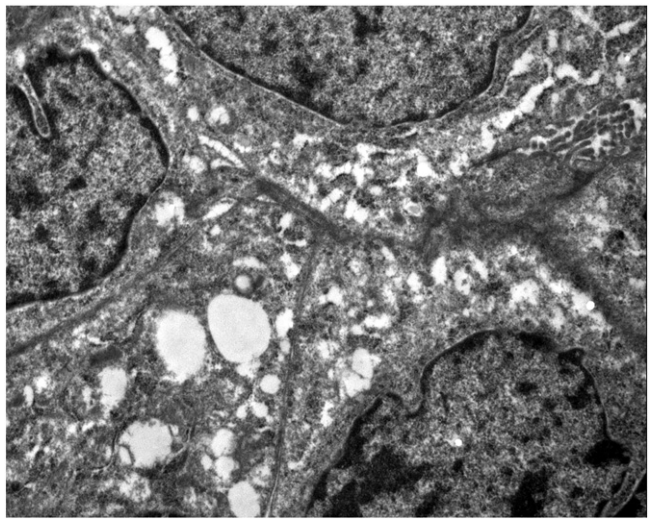

Fig. 12. Squamoid differentiation was confirmed ultrastructurally by the presence of desmosomes in the cytoplasm of the large tumor cell population.

The results of the molecular genetic study, which, for technical reasons, was performed on 1 case (no. 2) revealed complex genetic changes including partial or complete loss (*CDKN2A* locus) of genetic material on chromosomes 2, 5, 6, 9, 12, 15, 16, 17, 18, and 22. Also, gain of genetic material on chromosomes 1, 5, 11, 12, and 13 was documented. It is probable that these chromosomal changes affect many loci of tumor suppressor genes and oncogenes. Particularly, the previously mentioned biallelic loss of *CDKN2A* locus is a commonly observed feature in many types of cancer including RCC [8,9]. However, this pattern of genetic changes is highly unusual for any known neoplastic entity in renal pathology and further strengthens the impression that this may be a new, albeit extremely rare, variant of RCC. Chromosomal numerical aberrations in urothelial carcinomas are complex and heterogenous. Hence, it is not possible to establish any characteristic combination that can serve as a diagnostic correlate. Losses of 2q, 5q, 8p, 9, 10q, 11p, 18q, and Y and gains of 1q, 5p, 8q, and 17q have been described [10]. However, data are conflicting and some investigators have reported gains of chromosome 1, 7, 9, and X [11,12].

Most kidney tumors with squamous differentiation are of urothelial origin [4,13,14]. Our tumors showed no evidence of urothelial differentiation, and both tumors were strictly located

Table 2
Array CGH (aCGH) examination

Case	aCGH changes–loss(−)/gain(+)–cytoband	aCGH changes–nucleotide position (build: HG18/NCBI 36)	LOH confirmation markers
Case 1	NA	NA	NA
Case 2	+1q21.2-q42.13	148 149 999–225 249 999	D1S249, D1S213, D1S2878, D1S498
	−2q32.1-q32.3	184 549 999 to 196 849 999	
	−2q35	215 749 999 to 216 749 999	
	−5p14.3	21 349 999–21 549 999	
	+5q31.3-qter	140 749 999–180 649 999	D5S422, D5S400, D5S408, D5S436, D5S410, D5S2011, D5S2090, D5S1960
	−5q13.2	68 949 999–69 249 999	
	−6p12.3-p21.1	42 149 999–46 949 999	D6S1650, D6S282
	−6p22.1	26 849 999–27 049 999	
	−6q11.1-qter	62 749 999 to 170 844 488	D6S262, D6S264, D6S287, D6S434, D6S460, D6S462
	−9p13.2-p21.3	20 949 999–21 749 999 21 849 999–24 549 999 (biallelic) 24 649 999–37 649 999	D9S161, D9S1817, D9S169, D9S259, D9S1874
	+11p15.4-pter	49 999–4 649 999	D11S4046
	+12p13.31-p13.32	3 249 999–8 149 999	D12S99
	−12q23.1	97 749 999–97 849 999	
	+13q12.11	19 449 999–19 749 999	
	−15q11.2	20 749 999–20 949 999	
	−16q11.2-qter	45 049 999–88 806 636	D16S503, D16S3091, D16S415, D16S3040, D16S514, D16S3066
	−17p11.2-pter	49 999–21 549 999	D17S1852, D17S799, D17S921, D17S1791, D17S1828
	−18	49 999–76 107 910	D18S70, D18S474, D18S53
	−22q11.21	17 049 999–17 249 999	
	−22q13.1	37 249 999–37 349 999	

In some changes, no informative markers or none at all were found; thus, these changes stayed unconfirmed by LOH analysis. NA, not analyzable.

in the cortex with no anatomical relation to the medulla or pelvicalyceal system. Although coexpression of CK7 and CK20 is frequently encountered in urothelial neoplasms, uroplakin 3 and both p63 and p53 were completely negative. Although coexpression of CK7 and CK20 was noted in the large squamoid cells while the small cell component was completely negative. We are not aware of any study in the English literature that describe any urothelial lesion with the distinctly biphasic light microscopical appearance of the neoplastic cells and their organoid arrangements as seen in these renal tumors. Moreover, of the 10 chromosomes that showed losses in the analyzed case, only 3 of those occurred in any of the 8 chromosomes that most frequently exhibit losses in invasive urothelial carcinoma.

For obvious reasons (pertaining to site, morphology, and immunohistochemical features), the tumors presented herein should not be mistaken for the rare squamous cell carcinoma or (even rarer) adenosquamous carcinoma of the renal pelvis [4,13,15-18].

In addition, neither the histologic features nor the immunohistochemical findings are consistent with a teratomatous or any other germ-cell tumors [19]. Lastly, none of the 2 patients had or developed any other primary tumors. Hence, the rare occurrence of a metastasis (or even rarer; tumor to tumor metastasis) to the kidneys is highly unlikely in these cases [20].

The prominent alveolar pattern seen in these tumors is reminiscent of what may be encountered in some translocation RCCs and we have also seen this in an unusual “translocation/like“ renal tumor that occurred synchronously with a conventional clear cell RCC in a patient with germ-line *VHL* mutation in a 34-year-old woman [21]. However, in neither translocation carcinomas nor the translocation-like tumor did the neoplastic cells display such a biphasic appearance, which is a highly characteristic feature in tumors presented in this study. Moreover, as mentioned earlier, there was no immunoreactivity detected for HMB-45 or TFE3, no tumor cells with voluminous clear cytoplasm, and no pseudorosettes composed of lymphocyte-like cells arranged around globular

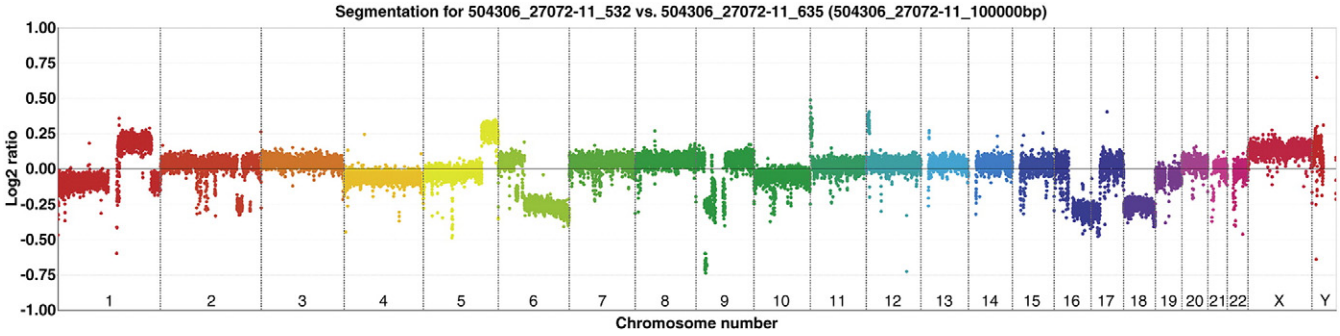

Fig. 13. Analysis of the neoplastic tissue of case 2 by array CGH revealed losses on chromosomes 2, 5, 6, 9, 12, 15,16, 17, 18, and 22, including biallelic loss of CDKN2A locus, and gains on chromosomes 1, 5, 11, 12, and 13.

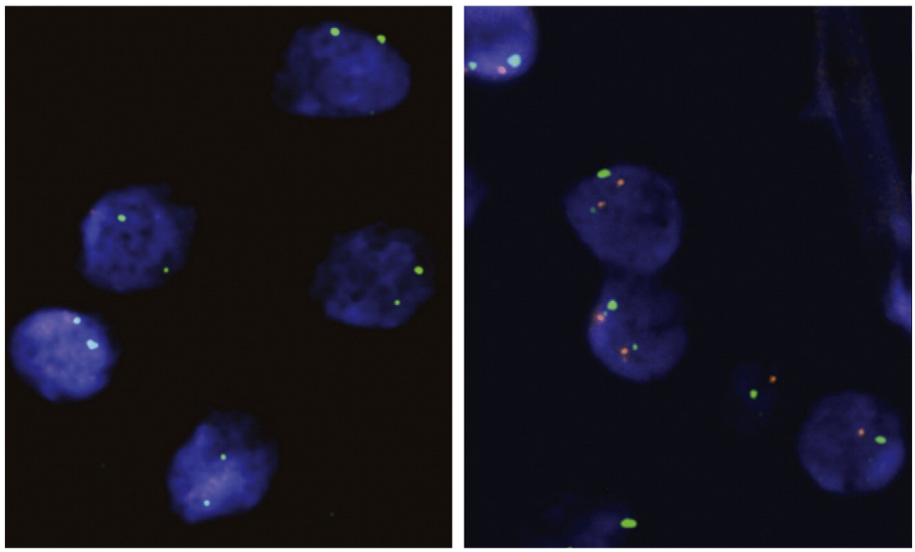

Fig. 14. Fluorescent in situ hybridization analysis confirmed biallelic loss in cytoband 9p21.3 where CDKN2A is located (45% [100]) in the neoplastic tissue from case 2 (left). In nontumor tissue, a normal signal pattern was observed (right).

cores of basement membrane material as seen in t(X;17); *TFE3* and t(6;11); *TFEB* renal carcinomas, respectively.

The squamoid appearance of the large tumor cells was supported by the diffuse expression of CK5/6 and the presence of desmosomes and tonofilaments in the ultrastructural study. However, we did not identify definitive morphologic proof of full squamous differentiation on light microscopy (intercellular bridges and/or keratin pearl formation). Also, immunohistochemically, the absence of nuclear expression of p63 is in line with the light microscopical impression, that is, with "squamoid" rather than complete squamous differentiation. Notwithstanding this fact, this appearance in a bona fide renal neoplasm with no evidence of sarcomatoid (de-) differentiation is a highly unusual feature that, we believe, may represent a new, albeit extremely rare and heretofore not reported type of RCC.

Despite finding a small focus of papillary architecture in case 1, there is very little probability that these tumors belong to the group of papillary RCC. Firstly, this finding was only minute/focal, and the overwhelmingly predominant architecture in both tumors was solid—alveolar and with a distinct biphasic composition of tumor cells. Secondly, both tumors were completely negative for vimentin, and the genetically analyzed case (case 2) did not show trisomy or polysomy of chromosomes 7 or 17 [22].

An interesting morphologic feature was encountered in case 2. There were small foci of intermediate-sized oncocyte-like cells arranged in small alveolated nests and some sheets. These oncocyte-like cells were surrounded by a loose, edematous connective tissue stroma. However, the immunohistochemical profile is not compatibile with that of renal oncocytoma (despite the relatively prominent expression of MIA). Moreover, the numerical chromosomal aberrations found in this case strongly argue against an oncocytoma. However, taken in isolation and just based on the light microcopical appearance, the resemblance to a bona fide oncocytomatous component was substantial.

In summary, (1) "biphasic alveolosquamoid renal carcinoma" appears to be a unique and distinctive tumor. (2) These tumors have a consistent immunohistochemical profile (positivity for CK7 and EMA in both the small and large cell components and diffuse immunoreactivity for CK 20 and CK5/6 in the large cell component) and with negative expression of many proteins commonly present in other known types of RCC. The large squamoid and small tumor cells have overlapping but distinctive patterns of immunohistochemically detectable protein expression. (3) Multiple chromosomal aberrations were identified, some of them located in regions with known tumor suppressor genes and oncogenes. (4) Further studies of a larger cohort of patients are warranted to elucidate the full spectrum of clinical behavior of these extremely rare but morphologically distinct renal neoplasms.

References

[1] Viswanathan S, Desai SB, Prabhu SR, et al. Squamous differentiation in a sarcomatoid chromophobe renal cell carcinoma: an unusual case report with review of the literature. Arch Pathol Lab Med 2008;132:1672-4.

[2] Mete O, Kilicaslan I, Ozcan F, et al. Sarcomatoid chromophobe renal cell carcinoma with squamous differentiation. Pathology 2007;39:598-9.

[3] van Dongen JJ, Langerak AW, Bruggemann M, et al. Design and standardization of PCR primers and protocols for detection of clonal immunoglobulin and T-cell receptor gene recombinations in suspect lymphoproliferations: report of the BIOMED-2 Concerted Action BMH4-CT98-3936. Leukemia 2003;17:2257-317.

[4] Mardi K, Kaushal V, Sharma V. Rare coexistence of keratinizing squamous cell carcinoma with xanthogranulomatous pyelonephritis in

the same kidney: report of two cases. J Cancer Res Ther 2010;6: 339-41.
[5] Workman C, Jensen LJ, Jarmer H, et al. A new non-linear normalization method for reducing variability in DNA microarray experiments. Genome Biol 2002;3 research0048.
[6] Larson PS, de las Morenas A, Bennett SR, et al. Loss of heterozygosity or allele imbalance in histologically normal breast epithelium is distinct from loss of heterozygosity or allele imbalance in co-existing carcinomas. Am J Pathol 2002;161:283-90.
[7] Martignoni G, Pea M, Gobbo S, et al. Cathepsin-K immunoreactivity distinguishes MiTF/TFE family renal translocation carcinomas from other renal carcinomas. Mod Pathol 2009;22:1016-22.
[8] Rocco JW, Sidransky D. p16(MTS-1/CDKN2/INK4a) in cancer progression. Exp Cell Res 2001;264:42-55.
[9] Strefford JC, Stasevich I, Lane TM, et al. A combination of molecular cytogenetic analyses reveals complex genetic alterations in conventional renal cell carcinoma. Cancer Genet Cytogenet 2005;159:1-9.
[10] Eble JN, Sauter G, Epstein JI. World Health Organization classification of tumours. Pathology and genetics. Tumours of the urinary system and male genital organs. Lyon: IARC Press; 2004.
[11] Sauter G, Simon R, Bubendorf L, et al. Molecular genetics of urinary bladder cancer progression. Verh Dtsch Ges Pathol 2002;86:49-56.
[12] Yu DS, Chen HI, Chang SY. Chromosomal aberrations in transitional cell carcinoma: its correlation with tumor behavior. Urol Int 2002;69: 129-35.
[13] Bhaijee F. Squamous cell carcinoma of the renal pelvis. Ann Diagn Pathol 2012;16:124-7.
[14] Zainuddin MA, Hong TY. Primary renal adenosquamous carcinoma. Urol Annu 2010;2:122-4.
[15] Howat AJ, Scott E, Mackie DB, et al. Adenosquamous carcinoma of the renal pelvis. Am J Clin Pathol 1983;79:731-3.
[16] Imbriaco M, Iodice D, Erra P, et al. Squamous cell carcinoma within a horseshoe kidney with associated renal stones detected by computed tomography and magnetic resonance imaging. Urology 2011;78: 54-5.
[17] Lee TY, Ko SF, Wan YL, et al. Renal squamous cell carcinoma: CT findings and clinical significance. Abdom Imaging 1998;23:203-8.
[18] Sovrea A, Vasiu R, Raica M, et al. Unusual renal carcinoma with a double component: case report and review of the literature. Rom J Morphol Embryol 2009;50:125-8.
[19] Otani M, Tsujimoto S, Miura M, et al. Intrarenal mature cystic teratoma associated with renal dysplasia: case report and literature review. Pathol Int 2001;51:560-4.
[20] Altinok G, Guler G, Sahin A. Tumor metastasis to an oncocytoma. Scand J Urol Nephrol 1999;33:416-7.
[21] Petersson F, Michal M, Vanecek T, et al. Bilateral renal tumors; conventional clear cell carcinoma and contralateral t(6;11)/t(X;17)-like tumor. Histomorphologic, immunohistochemical, ultrastructural and molecular genetic studies including the report of a novel mutation in the VHL gene. Ann Diagn Pathol 2011;15:362-9.
[22] Brunelli M, Eble JN, Zhang S, et al. Gains of chromosomes 7, 17, 12, 16, and 20 and loss of Y occur early in the evolution of papillary renal cell neoplasia: a fluorescent in situ hybridization study. Mod Pathol 2003;16:1053-9.